Environmental Science
Water Research & Technology

Energy Recovery in Capacitive Deionization Systems with Inverted Operation Characteristics

Journal:	*Environmental Science: Water Research & Technology*
Manuscript ID	EW-ART-09-2019-000797.R1
Article Type:	Paper

Water impact

Freshwater scarcity across the world is becoming a severe problem due to increasing population and anthropogenic activities. In consideration of the rising cost of energy, water treatment strategies must be energy-efficient. In this work, a Ćuk dc-dc converter effectively transfers the energy stored from one inverted capacitive deionization to another, aiding in deploying an energy-efficient brackish water treatment solution.

Energy Recovery in Capacitive Deionization Systems with Inverted Operation Characteristics

Ayokunle Omosebi[a*], Zhiao Li[b], Nicolas Holubowitch[c], Xin Gao[a], James Landon[ad], Aaron Cramer[e], and Kunlei Liu[af*]

[a]Center for Applied Energy Research, University of Kentucky, Lexington KY 40511, USA

[b]Department of Electrical Engineering, Tsinghua University, Beijing PRC

[c]Department of Physical and Environmental Sciences, Texas A&M University, Corpus Christi, TX 78412

[d]Department of Chemical and Materials Engineering, University of Kentucky, Lexington, KY 40506, USA

[e]Department of Electrical and Computer Engineering, University of Kentucky, Lexington, KY 40506, USA

[f]Department of Mechanical Engineering, University of Kentucky, Lexington, KY 40506, USA

*: Ayokunle.omosebi@uky.edu

*: Kunlei.Liu@uky.edu

Abstract

Capacitive deionization (CDI) operated under inverted mode involves electronic charging and discharge steps with corresponding ion concentration and desalting coupled with simultaneous energy storage. In this work, an energy recovery system derived from a Ćuk

dc-dc converter is explored to transfer the energy stored from one inverted capacitive deionization (i-CDI) cell during the electronic discharge step to another during the charge step, decreasing the overall energy requirement for capacitive water desalination. The i-CDI cell, a subset of CDI architecture operated in invert mode, is improved by incorporating ion-selective membranes to form inverted membrane capacitive deionization (i-MCDI), leading to enhanced charge storage achieved with reduced energy input. For example, in comparison to i-CDI that requires ~12 J/g of energy input, the i-MCDI cell requires only 8 J/g. By incorporating the recovery system, the energy penalty can be reduced to only require ~8 and 4 J/g for i-CDI and i-MCDI cells, respectively. Improvement in energy recovery was shown to be achieved by reducing charge leakage, with the i-MCDI cell showing up to 3 times the leakage resistance of the i-CDI cell.

1. Introduction

Capacitive deionization (CDI) is an emerging water treatment technique that shows great potential for ameliorating the effects of water scarcity due to its projected low energy requirements,[1, 2] suitability for selective ion removal,[3, 4] and ease of use in remote locations.[5] CDI uses modest potentials to electrostatically remove ionic species from a process stream, storing them temporarily in highly porous electrodes made up of a conductive, usually carbonaceous material.[6-10] When an electric potential is applied, ions are attracted to electrodes of the opposite polarity, forming an electric double layer, and storing the electrostatic potential energy for later use. When the electrodes become saturated, reducing the electric potential, or merely short-circuiting the electrodes facilitates the creation of a concentrate stream as both the adsorbed ions and their electrostatic potential are released from the electrodes in this step. A CDI cell is essentially

a desalination capacitor, and in the same manner as a capacitor, the accumulated electrostatic potential in the system can be recovered as direct current (dc) electricity during discharge to power auxiliary devices or coupled CDI units. However, CDI currently suffers from cyclability issues in large part due to electrode degradation, but methodologies for performance preservation in addition to energy recovery can make the technology more attractive.

In order to circumvent the shortcomings of conventional capacitive deionization, inverted capacitive deionization (i-CDI) was demonstrated where deionization was accomplished by the polarity difference between chemical surface charges on electrode pairs that in-turn facilitated the adsorption of counter ions from solution (Figure 1a). For discharge (Figure 1b), external electronic charge is added to balance the surface charge, thereby expelling previously adsorbed ions to migrate back to the bulk solution, forming an ion-rich stream.[11-14] Summarily, the i-CDI configuration was shown to (a) significantly extend the operational lifetime of the deionization operation beyond the capabilities of conventional CDI, (b) fundamentally depend on the separation between the potential of zero charge (E_{PZC}) of the electrodes of the anode-cathode pair such that performance increases with surface charge/E_{PZC} separation, and (c) less than unity charge efficiencies can be attributed to faradaic charge leakage combined with cell operation beyond the potential window created by the surface charge/E_{PZC} differential.[11] Also, unlike short-lived CDI, where the electronic charge is recovered from electrons previously balancing ions in solution, for i-CDI, the electronic charge is recovered from electrons previously balancing surface charges. Since the aforementioned inefficiencies of the i-CDI configuration will result in possibly poor energy recovery scenarios, we attempt to mitigate these deficiencies via

inverted membrane-assisted capacitive deionization (i-MCDI) (Figure 1c and d).[15] The i-MCDI cell leverages the i-CDI architecture[11] as well as the property of ion-selective membranes to effect enhanced salt storage while minimizing parasitic charge losses.[16-18] In this work, the recovery of energy between two interconnected i-CDI or i-MCDI cells is mechanistically explored.

Using recovered energy from a discharging i-CDI cell to power subsequent i-CDI cells leads to even lower energy consumption for the desalination process. While a significant portion of CDI literature has focused on materials development and cell optimization, only a numbered few have focused on energy recovery methods. These methods include directly connecting two cells,[19] discharging a pre-charged CDI cell over a load,[20-22] transferring energy from a CDI cell to a supercapacitor using a buck-boost dc-dc converter,[2] and recovery from membrane CDI to supercapacitor via a buck-boost converter.[23] Energy recovery from CDI is temporal at best due to energy lost to cell degradation under the applied potential, and although the buck-boost topology is simple, it draws pulsed currents from the source and provides pulsed currents to the load and has relatively high switching losses.[24] These currents will either increase the electrical losses in the cells and diminish cell performance due to electrode oxidation and un-matched the potential of zero charge, or they must be filtered out with large inductive-capacitive filters that lead to slow dynamic response and increased losses. In this work, a dc-dc converter system derived from a Ćuk topology is used to facilitate energy transfer between two i-CDI cells. The Ćuk topology applies pulsed voltages to the source and the load, which can be modulated to carefully control the current flowing in and out of the cells with only a simple inductive filter. Unlike the buck-boost, the Ćuk converter incorporates a power supply that compensates for energy

losses during the transfer process, thereby allowing the system to simultaneously meet its desalination goals during the transfer process.[25] In this work, the efficacy of a converter derived from a Ćuk topology for cell-to-cell energy transfer will be explored as a means to reduce desalination energy consumption. A mathematical circuit model is included to describe the energy recovery process and provide comparative results for both i-CDI and i-MCDI cells.

2. Experimental

2.1 Deionization cell assembly

The i-CDI cell is made up of a sequential stack of current collector, anode (+), spacer channel, cathode (-), and current collector (Figure 1a,b). The current collectors were ~1 mm thick titanium plates, while the spacer channel was a ~2 mm sandwich structure composed of two silicone rubber gaskets on either side of a filter paper separator. Spectracarb 2225 Type 900 activated carbon fabric (Engineered Fibers Technology, LLC) was used as porous electrodes. The cathode was pristine as-received Spectracarb (SC-Pr), while the anode was nitric acid oxidized Spectracarb (SC-Ox). The electrode treatment process comprised of soaking the SC-Pr substrate in 60 wt% HNO_3 for 24 hours, followed by repeated rinsing with DI water until the solution pH became neutral, and then drying in a convection oven preset at 100 ºC. The SC-Pr and SC-Ox electrodes have been previously shown to respectively possess positive and negative surface charges that attract anions and cations in solution, thus facilitating i-CDI operation.[26, 27] For the i-MCDI cell, ~175 um thick ion-exchange Neosepta AMX and CMX membranes were respectively added to the cathode and anode to form a new structure with a current collector, anode (SC-Ox), CMX, spacer channel, AMX, cathode (SC-Pr) and current collector sequential stack (Figure 1c,d).

The AMX and CMX membranes selectively transport anions and cations, respectively, and it should be noted that their locations in the cell assembly are also inverted in comparison to conventional MCDI cells where the AMX would be placed next to the anode and the CMX next to the cathode. A total carbon electrode mass of ~1.9 and 2.1 g of carbon was used to form the i-CDI and i-MCDI cells, respectively.

2.2 Test System

The test system consisted of either an i-CDI or i-MCDI cell, solution reservoir, power source, energy recovery system, and sensors (Figure 2). Deionization experiments were carried out in two modes (control with a single cell and recovery with dual cells) by circulating 18.5 L of ~10 mM NaCl solution contained in a reservoir through a deionization cell using a peristaltic pump (Cole-Parmer Masterflex L/S) at ~14 ml/min. The large reservoir facilitates quasi-single pass operation. An in-line conductivity sensor was connected to the exits of the deionization cells to track changes in conductivity. Cell 1 (plus Cell 2 in recovery mode) and the power supply current and voltages were simultaneously tracked during the experiments, and all sensors (including conductivity) were connected to a Graphtec midi logger GL220 programmed to nominally obtain and log data at a rate of 1 Hz. There was no purging of N_2 or Ar during testing in order to simulate energy recovery in a real-world scenario.

2.2.1 Characterization Mode

In characterization mode, the performance of the i-CDI or i-MCDI cell was evaluated by charging at 1.2 V (Circuit Specialists 3644 A) and short-circuiting the electrode leads to discharge the cell. Each charge or discharge cycle lasted for 1 hour. The ionic charge density (Q_{ion}) during charging/discharging of the carbon electrodes in each i-CDI or i-

MCDI was determined from the integral of the concentration profile converted to equivalent charge normalized by the total mass of electrodes (equation 1).

$$Q_{ion} = \frac{A\phi F}{m}\int_0^t [\sigma(t) - \sigma_s]dt \quad (1)$$

where σ(t) and σ_s are transient and steady-state conductivity, and *F*, A, ϕ, and m are Faraday's constant, calibration parameter (8.87 x10^{-6} mol-cm/L-μS), flow rate of the salt solution, and mass of the electrode, respectively. The electronic charge density Q_e is computed from the integral of the electric current normalized by the electrode mass, and the energy consumed to facilitate charge transfer (E_{PS}) is a product of the electronic charge density and applied potential (V_{PS}), which is kept at 1.2 V in this work. The subscript PS denotes the power supply.

$$E_{PS} = \frac{V_{PS}}{m}\int_0^t idt \quad (2)$$

2.2.2 Energy Recovery Mode

In recovery mode, two structurally identical cells are always used. Prior to energy recovery, cell 1 is charged at a constant voltage, and once charged, the energy stored is then transferred to cell 2 via a microcontroller regulated converter. An electrical circuit diagram for the cell-to-cell recovery system is shown in Figure 3. Each cell-under-test is represented by a simplified Randles circuit, which is a resistor (charge leakage medium) and capacitor (storage medium) connected in parallel but both serially connected to a second resistor (charge transport medium). For example, cell 1 is composed of C_1, R_P, and R_S in Figure 3. The recovery system uses two metal oxide semiconductor field-effect transistors (MOSFET) as switches (SW_1, SW_2), three inductors (L_1, L_2, and L_f in Figure 3), and one

capacitor (C_f) as energy transfer media. The use of the MOSFET for switching elements makes bidirectional operation possible. The inductor L_f placed between the power supply and C_f filters current flowing from the power supply, substantially reduces the likelihood of current flowing in reverse to the power supply, and limits the power supply's ripple current. The converter operates in a series of steps to transfer energy from the capacitive element of cell 1 (C_1) to that of cell 2 (C_2). With C_1 already charged, MOSFET switch SW_1 is closed, and current flows from C_1 to be temporarily stored in the inductor L_1. Then, SW_1 is opened, SW_2 is closed, and current continues to flow through L_1, transferring charge to capacitor C_f. While SW_1 is closed, SW_2 is open, therefore the transfer capacitor discharges through L_2 and creates a current flow to charge C_2. The MOSFET switching frequency is 20 kHz.

The actual charge/discharge operation with the converter involves regulating duty cycles D_1 and D_2, which represent the on-times for the two MOSFET switches, SW_1 and SW_2, in one period. Since D_1 and D_2 are complementary such that if D_1 is 1 (SW_1 closed) then D_2 is 0 (SW_2 is open), then $D_2 = 1\text{-}D_1$. The duty cycle is regulated by the microcontroller to achieve the required charging and discharging operations. To charge cell 1 at a constant voltage, current flows from the power supply to C_1, by respectively maintaining D_1 and D_2 as 0 and 1. During energy transfer, the cell voltages are linearly ramped. For example, for the ramped discharging of C_1 and charging of C_2, D_1 increases linearly from 0 to 1 as D_2 increases from 1 to 0. As a result, energy is transferred from C_1 to C_2, causing corresponding linearly decreasing and increasing voltages in C_1 and C_2, respectively. To evaluate energy recovery, the energy required to charge a cell is considered with and without the recovery process. Therefore, the fractional energy recovery, r, on the basis of

the quantity of ionic charge transferred is defined to be the difference between the total energy provided by the power supply to charge the cell with and without the recovery system, normalized by the energy without the recovery system.

$$r = \frac{E_{PS}|_{No\ Recovery} - E_{PS}|_{Recovery}}{E_{PS}|_{No\ Recovery}} \quad (2)$$

3. Model Derivation

A model is presented for the energy recovery system based on the electrical circuit in Figure 3. The model provides a platform for observing the impact of the circuit elements in the converter system on energy transfer between the connected cells and for scale-up of the system to transfer more energy if required. In order to construct the recovery system, the circuit elements (L_f, C_f, SW_1, SW_2, L_1, L_2, and R_{SR}) are chosen to optimize the transfer process and provide consistent voltage and current profiles. It is essential that non-CDI resistances contributed by sensors, inductors, and switches be minimal, and therefore C_f should be capable of transferring energy in short-time scales, and inductors should have ripple currents less than 20% of the average inductor current. Inductors L_1 and L_2 have inductances of 2.2 mH and internal resistances of 0.8 Ohm. Inductor L_f has an inductance of 1 mH and a resistance of 1 Ohm. The transfer capacitor (C_f) has a capacitance of 8.3 F, and the converter circuit is rated for a maximum current and voltage of 500 mA and 1.2 V, respectively. For the purpose of making energy calculations, the voltage and current status of each component in the CDI-converter system needs to be known, where the power provided by C_1 is V_1*i_1, by the power supply is V_{PS}* i_{Lf}, and to C_2 is V_2*i_2.

Model equations are obtained by applying Kirchhoff's voltage (KVL) and current (KCL) laws to circuit loops or nodes in Figure 3. The nodes of interest are numbered 1 through

12. For example, considering the loop formed by nodes 2, 3, 11 and 12, the current flowing to the first cell, i_1, can be described by

$$L\frac{di_1}{dt} = V_1 - i_1 * (R_{SR} + R_l) - V_{sw1} \quad (3)$$

Here R_{SR} and R_L are the resistances across sensors and inductors, respectively. V_1 is the voltage sensed between nodes 2 and 12, which is equivalent to the total voltage across cell 1. The voltages across the MOSFET switches SW_1 and SW_2 can be obtained from the loop formed by nodes 3, 6, 10, 11.

$$V_{sw1} = D_1 * i_{sw1} * R_{sw} + (1 - D_1) * (V_{cf} - V_{sw2}) \quad (4)$$

$$V_{sw2} = (1 - D_1) * i_{sw2} * R_{sw} + D_1 * (V_{cf} - V_{sw1}) \quad (5)$$

The current into the transfer capacitor can be obtained by considering node 3 where

$$C_f\frac{dV_{cf}}{dt} = i_{lf} + i_1 - i_{sw1} \quad (6)$$

By considering loop 3,4,5,6, the voltage across the transfer capacitor, V_{cf}, can be obtained according to

$$L_f\frac{di_{lf}}{dt} = V_{in} - V_{cf} - R_{lf} * i_{lf} \quad (7)$$

A complete list of equations along with initial conditions is provided in the SI. The electronic circuit for the cells and converter, including their corresponding differential equations and initial conditions were converted to a MATLAB Simulink™ model, and their solution was obtained using the ordinary differential equation package ODE23TB.

4. Results and Discussions

4.1 Energy recovery from a simulated dummy cell

There are several ways to recover energy from a discharging capacitor such as a CDI cell. The easiest way is to connect two CDI cells together. For the sake of simplicity, CDI cells are considered as ideal capacitors. Hence, for two CDI cells with total capacitance *C*, if one of the capacitors (denoted as Cap 1) is fully charged to voltage V_{IN}, the energy stored in that capacitor is $E = 0.5CV_{IN}^2$, and the charge stored is $Q = CV_{IN}$. When charged Cap 1 is connected to transfer its energy to Cap 2 (previously at 0 V), both cells will reach a final voltage V_f. Due to charge conservation, the charge initially on Cap 1 is divided equally between the two cells, $Q = C\ V_{IN} = 2CV_f$, and therefore V_f is one half of V_{IN}. Thus, the energy now stored in Cap 1 and Cap 2 are $E_1 = E_2 = 0.5CV_f^2 = 0.25E$. This indicates that the energy recovered in a cycle is only 25% when directly connecting two cells together, and from a deionization perspective the end result will be a partially discharged Cap 1 and a partially charged Cap 2, which will not satisfy the deionization requirements of the operation. In contrast, using a dc-dc converter can help move more charge from cell 1 into cell 2, and up to 80% energy recovery when transferring energy between two supercapacitors using a buck-boost converter has been demonstrated.[28] Since i-CDI cells are very similar to EDL supercapacitors, similar energy recovery should be possible, and in the following sections, converter-assisted energy transfer between two deionization cells will be presented.

Firstly, the model and energy recovery operations are implemented with an electrical dummy cell (EDC) connected to the recovery system. The EDC is made up of resistors and capacitors that represent cells 1 and 2. The C_1, C_2, R_P, and R_S components (Figure 3) have

corresponding values of 8.3 F, 8.3 F, 100 Ohm, and 15 Ohm, respectively. A picture of the EDC is provided in Figure S1. Values for the C_1, C_2, R_P, and R_S components of the EDC were approximately determined based on fitting results for a CDI cell to a Randles circuit. Similar analysis procedure can be found in Refs.[29, 30] Figure 4 shows the experimental (EDC) and simulated (Simulink™) voltage and current profiles for cells 1 and 2, and the power supply during the constant voltage (1.2 V) pre-charging and subsequent energy recovery periods. The pre-charging period lasts 600 s, followed by voltage regulation by the microcontroller to linearly reduce the voltage across cell 1, V_1, from 1.2 to 0 V over 600 s while V_2 simultaneously increases to 1.2 V during the same time interval. After t = 1200 s, the power supply solely powers cell 2 (constant voltage charging). There is generally good agreement between the simulated and experimental voltage profiles as shown in Figures 4a and b. It should be noted that when potential is initially applied to cell 1 during pre-charging, V_1 at the beginning of the experiment (t =0) is ~1 V which is less than V_{PS} due to parasitic voltage drop caused by resistances in the line, sensor (R_{SR}), and inductors (R_{Lf} and R_L). However, V_1 approaches V_{PS} as the impedance of the capacitor increases and current is forced through R_P, where R_P in addition to $R_S >> R_{SR}$, R_L, and R_{Lf}. Charging cell 1 with constant voltage results in a current spike that decays non-linearly to the steady-state current based on the values of R_S and R_P. No current is passed to cell 2 during this pre-charging period, and the power supply current is the same as the current for cell 1. During recovery (t > 600 s), the voltage across cell 1 decreases while the voltage across cell 2 increases, and the power supply voltage is always constant at 1.2 V. Cell 1 discharges, hence its current tends towards negative values, then relaxes to zero based on the voltage ramp profile. The current across cell 2 first increases, then decreases towards a

non-zero current (C_2 capacitor is filled followed by leakage current), while the current provided by the power supply first decreases towards 0, but then increases as more power is needed to charge cell 2.

As the microcontroller begins regulating the voltage across cell 1 to 0 using the duty cycle, the voltage loss across R_S (also a function of R_P such that increasing R_P minimizes this voltage loss) is instantaneously consumed and cannot be recovered, making the open circuit voltage at the capacitor V_{C1} less than V_1 at the onset of recovery at t = 600 s. Therefore, there is energy input to cell 1 (hatched regions in Figures 4 c and e) reflected by the positive current at the onset of recovery for cell 1, as well as the non-zero power supply current that slowly relaxes to zero. It is therefore necessary to force an initial voltage drop (such that $V_{C1} > V_1$) to prevent energy addition to C_1 at the onset of the recovery period, which is accomplished by D_1 modulation.

Figure 5 shows recovery results where an initial voltage drop of 0.3 V was first enforced at t = 600 s, before linear ramping. The experimental and simulated voltage and current profiles appear to match, and the instantaneous voltage drop in cell 1 at t = 600 s (Figure 5a) results in a voltage rise for cell 2 (Figure 5b). Here, the discharge current for cell 1 is immediately negative and there is an instantaneous current rise in cell 2. The power supply current is initially at zero (no parasitic consumption by cell 1) and increases as needed over the course of energy transfer from cell 1 to cell 2. Considering the two scenarios with voltage drops (V_{drop}) of 0 and 0.3 V, the 0.3 V leads to a more significant amount of energy stored per input from the power supply (Figure 5f), which is due to the more sluggish current response for Cell 2 for the 0 V drop. In addition to V_{drop}, it is expected that ramp

duration will also affect the power supply input requirement, since any voltage loss across R_S cannot be recovered and energy continually leaks from R_P.

Each combination of voltage drop and ramp time leads to a distinct voltage ramp rate. For example, the 0 V V_{drop} 600 s ramp time and 0.3 V V_{drop} 600 s ramp time combinations have voltage ramp rates of 2 and 1.5 mV/s, respectively. Figure 6 shows a simulation plot for the power supply requirement for cell 2 as a function of V_{drop} and ramp time. In summary, several scenarios can result in less than optimum power supply requirements. With a low voltage drop, differences in V_{C1} vs. V_1 at the onset of charging cause a parasitic power draw by cell 1, whereas at large V_{drop}, there is significant power dissipation across all of the serial resistors, which accounts for the preference of a slow charging rate or low constant current with regards to minimizing dissipated energy during charging.[31, 32] Nonetheless, constant voltage operation mode is still widely used for CDI operations. In Figure 6, at low ramp times, the operation approaches constant voltage operation, whereas at significant ramp times, the accumulated contributions of charge leakage via R_P can be significant. Of the conditions tested, the best point that minimizes the power supply input for charging cell 2 was a combination of a V_{drop} of ~0.3 V and a ramp time of ~500 s. It should be noted that for each combination of R_P, R_S, C, there will be an optimum power supply requirement as shown in Figure S2 and Table S1.

4.2 Performance of i-CDI and i-MCDI cells.

Based on the convention used in this work, current is positive during charging indicating external electronic charge input to the cell, and negative during discharge indicating electronic output from the cell. Figure 7a shows current profiles for the i-CDI and i-MCDI cells during performance (salt adsorption/desorption) cycling based on Figure 2a. The cells

were operated at 0/1.2 V to desalinate and concentrate the influent stream. Ideally low R_S (large initial current) and large R_P (small final current, minimized charge leakage) are desired as suggested by the optimization results in Figure S2 and the current profile deconvolution in Figure S3 for known values of R_S, R_P, and C. Comparing the i-CDI and i-MCDI cell currents, higher initial and final currents were observed for the i-CDI cell (~48 mA/g and ~7 mA/g) in comparison to the i-MCDI cell (~43 mA/g and ~2 mA/g). Given that the membranes provide facile transport of counter ions to/from their respective electrodes, the reduction in initial current for the i-MCDI cell is likely due to interfacial resistance where the membrane poorly contacts the electrode [33]. Based on the assumption that the current at the end of the charging phase approximates the charge leakage, then the i-CDI cell self-discharges by ~3 times the i-MCDI cell, and thus the i-CDI cell is expected to be comparatively less efficient for energy recovery operations. Randles circuit fitting of the current profiles (Figure S4) show C, R_S, and R_P values of 12 F, 15 Ohm, and 80 Ohm for the i-CDI cell, but 12 F, 17 Ohm, and 210 Ohm for the i-MCDI cell, with the most characteristic difference being the R_P values for the two cells, thus highlighting the impact of the membrane on suppressing charge leakage.

Figure 7b shows the corresponding conductivity (i.e., desalination) profiles for the i-CDI and i-MCDI current profiles shown in Figure 7a. Unlike conventional CDI cells, applied potential facilitates desorption rather than adsorption in i-CDI and i-MCDI, which implies that energy from the power supply is consumed only during the desorption step, and ions are adsorbed upon cell discharge at short-circuit. The observed conductivity profiles were typical of a single-pass mode of operation whereby the conductivity at the end of each cycle approaches the steady state conductivity values, and the area under the desorption

peak during charging or over the adsorption valley during discharging represents the quantity of salt desorbed or adsorbed. Additional detail on cycle to cycle performance is provided in Fig S5. Larger desorption/adsorption areas can be observed for the i-MCDI cell by inspection. The corresponding nominal ionic charge, Q_{ion} passed (cell 1 and 2) during the charging period were ~12 and ~15.0 C/g for the i-CDI and i-MCDI cells, respectively (Figure S6). The larger Q_{ion} for the i-MCDI cell is consistent with the expectation that the membranes minimize charge expulsion to improve deionization performance as is clearly evident in Figure 7c where a repulsion spike is observed for the i-CDI cell. Therefore, in addition to a larger steady state current, the performance of the i-CDI cell is also diminished by ion-expulsion at the operation voltage. Figure 7 also indicates that i-CDI operation is outside of its electrode self-generated potential window. Since i-CDI operation depends on the potential window created by the chemical charge/E_{PZC} separation ,[14, 34, 35] when a potential in excess of the potential window is applied, it leads to re-adsorption of ions during electronic charging/ion concentration. In response, during the electronic discharge/desalination step at 0 V, previously adsorbed ions at these potentials beyond the working window are first desorbed before ion storage can occur, e.g., Na^+ desorption before Cl^- adsorption at cathode. In contrast, the ion exchange membrane restricts transport of ions that are for responsible for re-adsorption during the electronic charge step which is an added benefit of i-MCDI operation.

4.3 Energy recovery from i-CDI and i-MCDI cells

Prior to energy recovery, cell 1 was charged to 1.2 V for 1000 s. During recovery, a 0.3 V V_{drop} was first applied, followed by linear discharge of the remaining voltage in cell 1 to 0 V over 600 s after which D_1 is maintained at 1 to charge cell 2 at constant voltage. The

choice of V_{drop} and ramp time was chosen based on R_P and R_S values, and optimization results in Figure S2. The voltage, current, and conductivity profiles for the i-CDI and i-MCDI cells during the recovery phase are shown in Figure 8a-f. The voltage profiles for cells 1 and 2 of the i-CDI and i-MCDI cells are similar (Figure 8a,d), thus indicating similar control characteristics by the recovery system. The value of the final current for cell 2 during charging of the i-CDI cell was ~6 mA/g, which is approximately 2-3 times the current for the i-MCDI (~3 mA/g). Also, larger conductivity response is observed for the i-MCDI cell (Figure 8c,f). The energy requirement for transferring an equivalent amount of ionic charge during charging is plotted in Figure 8g, and it is clearly evident that the recovery process leads to energy savings for both i-CDI and i-MCDI cells. For example, the energy requirement for the constant voltage transfer of 6 C/g of ionic charge for cell 2 of the i-CDI and i-MCDI cells were ~11 and 8 J/g, whereas with the recovery system, they only require ~8 and 4 J/g, respectively. Based on eqn. 3, for 8 C/g of ionic charge, there is a 50% recovery for the i-MCDI cell, but only 20% for the i-CDI cell, where recovery in the i-CDI cell is impacted by a greater degree of charge leakage. The results presented in Figures 5-8 implicate the recovery system as a useful tool for reusing the energy stored during capacitive-based desalination. Further enhancements in desalination performance can be achieved through the addition of membranes to the i-CDI cell while reducing energy input requirements.

5. Conclusions

For the first time, we present results for cell-to-cell energy recovery between two inverted capacitive deionization (i-CDI) cells, which were shown in recent work to possess significantly extended performance lifetimes in comparison to capacitive deionization

(CDI) cells. The recovery system utilizes a dc-dc converter based on a Ćuk design with an active power supply input to compensate for energy losses during the transfer process. The i-CDI cell architecture is improved to form an inverted membrane-assisted capacitive deionization (i-MCDI) cell that incorporates ion-selective membranes with the i-CDI cell structure, leading to enhanced charge storage achieved with reduced energy input. Operation of the i-CDI and i-MCDI cells to store 6 C/g of charge required ~ 12 and 8 J/g of energy when charging the cells at a constant potential of 1.2 V, respectively. However, by incorporating the recovery system, the energy penalty can be reduced to only require ~8 and 4 J/g for the i-CDI and i-MCDI cells, respectively. Energy recovery was shown to be improved by reducing charge leakage, with the i-MCDI cell showing up to 3 times the leakage resistance of the i-CDI cell. The capacitive deionization process can help relieve water scarcity problems that are increasing in communities around the globe and can also be more efficient with an energy recovery system in place, leading to lower energy requirements. Further research into materials that suppress charge leakage during charging while reducing ion-transport resistance can help improve the energy recovery process.

Conflict of interest

There are no conflict of interest to declare.

Acknowledgements

The authors are grateful to the U.S.−China Clean Energy Research Center, U.S. Department of Energy for project funding (No. DE-PI0000017). The authors also thank Mr. R. Perrone for help in designing and constructing the i-CDI and i-MCDI cells.

References

1. T. J. Welgemoed and C. F. Schutte, Capacitive Deionization Technology™: An alternative desalination solution, *Desalination*, 2005, **183**, 327-340.
2. M. Alkuran, M. Orabi and N. Scheinberg, 2008.
3. L. Wang and S. Lin, Mechanism of Selective Ion Removal in Membrane Capacitive Deionization for Water Softening, *Environmental Science & Technology*, 2019, **53**, 5797-5804.
4. E. N. Guyes, T. Malka and M. E. Suss, Enhancing the Ion-Size-Based Selectivity of Capacitive Deionization Electrodes, *Environmental Science & Technology*, 2019, **53**, 8447-8454.
5. M. E. Suss, S. Porada, X. Sun, P. M. Biesheuvel, J. Yoon and V. Presser, Water desalination via capacitive deionization: what is it and what can we expect from it?, *Energy & Environmental Science*, 2015, DOI: 10.1039/C5EE00519A.
6. J. C. Farmer, D. V. Fix, G. V. Mack, R. W. Pekala and J. F. Poco, Capacitive deionization of NaCI and NaNO3 solutions with carbon aerogel electrodes, *Journal of the Electrochemical Society*, 1996, **143**, 159-169.
7. M. Andelman, Flow through capacitor basics, *Separation and Purification Technology*, 2011, **80**, 262-269.
8. S. Porada, R. Zhao, A. van der Wal, V. Presser and P. M. Biesheuvel, Review on the science and technology of water desalination by capacitive deionization, *Progress in Materials Science*, 2013, **58**, 1388-1442.
9. J. J. Lado, R. E. Pérez-Roa, J. J. Wouters, M. Isabel Tejedor-Tejedor and M. A. Anderson, Evaluation of operational parameters for a capacitive deionization reactor employing asymmetric electrodes, *Separation and Purification Technology*, 2014, DOI: http://dx.doi.org/10.1016/j.seppur.2014.07.004.
10. M. E. Suss, S. Porada, X. Sun, P. M. Biesheuvel, J. Yoon and V. Presser, Water desalination via capacitive deionization: what is it and what can we expect from it?, *Energy Environ. Sci.*, 2015, **8**, 2296-2319.
11. X. Gao, A. Omosebi, J. Landon and K. Liu, Surface charge enhanced carbon electrodes for stable and efficient capacitive deionization using inverted adsorption-desorption behavior, *Energy & Environmental Science*, 2015, **8**, 897-909.
12. P. Biesheuvel, M. Suss and H. Hamelers, Theory of water desalination by porous electrodes with fixed chemical charge, *arXiv preprint arXiv:1506.03948*, 2015.
13. X. Gao, A. Omosebi, J. Landon and K. Liu, Voltage-Based Stabilization of Microporous Carbon Electrodes for Inverted Capacitive Deionization, *The Journal of Physical Chemistry C*, 2018, **122**, 1158-1168.
14. T. Wu, G. Wang, F. Zhan, Q. Dong, Q. Ren, J. Wang and J. Qiu, Surface-treated carbon electrodes with modified potential of zero charge for capacitive deionization, *Water Research*, 2016, **93**, 30-37.
15. P. A. Fritz, R. M. Boom and K. Schroen, Polyelectrolyte-activated carbon composite electrodes for inverted membrane capacitive deionization (iMCDI), *Separation and Purification Technology*, 2019, **220**, 145-151.

16. P. M. Biesheuvel, R. Zhao, S. Porada and A. van der Wal, Theory of membrane capacitive deionization including the effect of the electrode pore space, *Journal of Colloid and Interface Science*, 2011, **360**, 239-248.
17. A. Omosebi, X. Gao, J. Landon and K. Liu, Asymmetric electrode configuration for enhanced membrane capacitive deionization, *ACS applied materials & interfaces*, 2014, **6**, 12640-12649.
18. J.-H. Choi, Determination of the electrode potential causing Faradaic reactions in membrane capacitive deionization, *Desalination*, 2014, **347**, 224-229.
19. J. Landon, X. Gao, J. K. Neathery and K. Liu, Energy Recovery in Parallel Capacitive Deionization Operations, *ECS Transactions*, 2013, **53**, 235-243.
20. O. N. Demirer, R. M. Naylor, C. A. Rios Perez, E. Wilkes and C. Hidrovo, Energetic performance optimization of a capacitive deionization system operating with transient cycles and brackish water, *Desalination*, 2013, **314**, 130-138.
21. L. Han, K. Karthikeyan and K. B. Gregory, Energy Consumption and Recovery in Capacitive Deionization Using Nanoporous Activated Carbon Electrodes, *Journal of The Electrochemical Society*, 2015, **162**, E282-E288.
22. L. Wang, J. E. Dykstra and S. Lin, Energy Efficiency of Capacitive Deionization, *Environmental Science & Technology*, 2019, **53**, 3366-3378.
23. J. Kang, T. Kim, H. Shin, J. Lee, J.-I. Ha and J. Yoon, Direct energy recovery system for membrane capacitive deionization, *Desalination*, 2016, **398**, 144-150.
24. A. A. Fardoun, E. H. Ismail, A. J. Sabzali and M. A. Al-Saffar, Bidirectional converter for high-efficiency fuel cell powertrain, *Journal of Power Sources*, 2014, **249**, 470-482.
25. S. Cuk and R. Middlebrook, 1977.
26. X. Gao, A. Omosebi, J. Landon and K. Liu, Enhanced Salt Removal in an Inverted Capacitive Deionization Cell Using Amine Modified Microporous Carbon Cathodes, *Environmental Science & Technology*, 2015, DOI: 10.1021/acs.est.5b02320.
27. X. Gao, S. Porada, A. Omosebi, K. L. Liu, P. M. Biesheuvel and J. Landon, Complementary surface charge for enhanced capacitive deionization, *Water Res.*, 2016, **92**, 275-282.
28. A. M. Pernia, J. G. Norniella, J. A. Martin-Ramos, J. Diaz and J. A. Martinez, Up-Down Converter for Energy Recovery in a CDI Desalination System, *Power Electronics, IEEE Transactions on*, 2012, **27**, 3257-3265.
29. S. Ban, J. Zhang, L. Zhang, K. Tsay, D. Song and X. Zou, Charging and discharging electrochemical supercapacitors in the presence of both parallel leakage process and electrochemical decomposition of solvent, *Electrochimica Acta*, 2013, **90**, 542-549.
30. A. Omosebi, X. Gao, J. Landon and K. Liu, Membrane Assisted Capacitive Deionization with Binder-Free Carbon Xerogel Electrodes, *ECS Transactions*, 2014, **61**, 9-17.
31. R. Zhao, P. M. Biesheuvel and A. van der Wal, Energy consumption and constant current operation in membrane capacitive deionization, *Energy & Environmental Science*, 2012, **5**, 9520-9527.

32. J. Kang, T. Kim, K. Jo and J. Yoon, Comparison of salt adsorption capacity and energy consumption between constant current and constant voltage operation in capacitive deionization, *Desalination*, 2014, **352**, 52-57.
33. P. Długołęcki and A. van der Wal, Energy Recovery in Membrane Capacitive Deionization, *Environmental Science & Technology*, 2013, **47**, 4904-4910.
34. X. Gao, S. Porada, A. Omosebi, K. Liu, P. M. Biesheuvel and J. Landon, Complimentary Surface Charge for Enhanced Capacitive Deionization, *Water Research*, 2016, DOI: 10.1016/j.watres.2016.01.048.
35. I. Cohen, E. Avraham, Y. Bouhadana, A. Soffer and D. Aurbach, Long term stability of capacitive de-ionization processes for water desalination: The challenge of positive electrodes corrosion, *Electrochim. Acta*, 2013, **106**, 91-100.

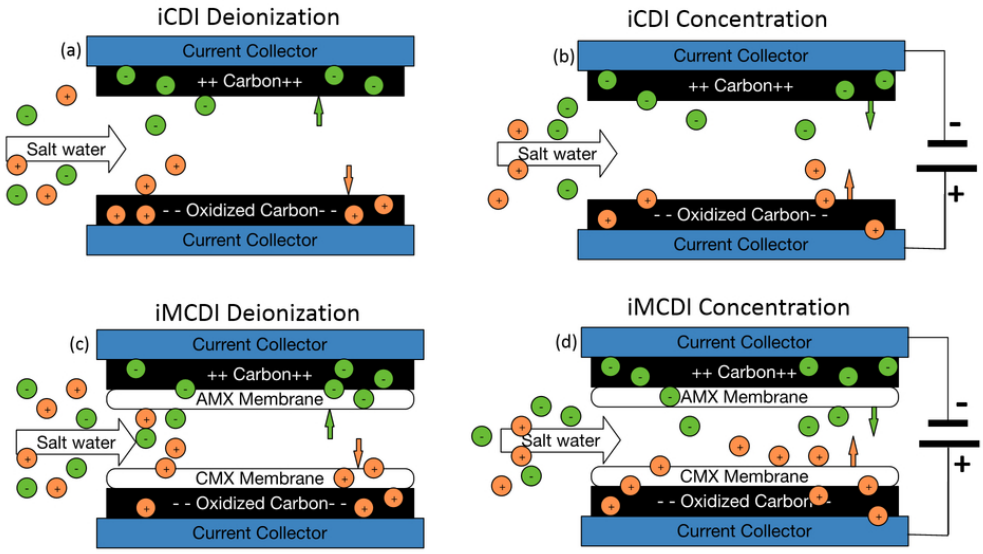

Figure. 1 Schematic representation of deionization and concentration operations in i-CDI and i-MCDI cells. Deionization is facilitated by chemical charges on the carbon electrodes, and concentration is achieved by applying an external electric potential. The incorporation of the ion-selective membranes enhances electrosorption of ions.

80x45mm (300 x 300 DPI)

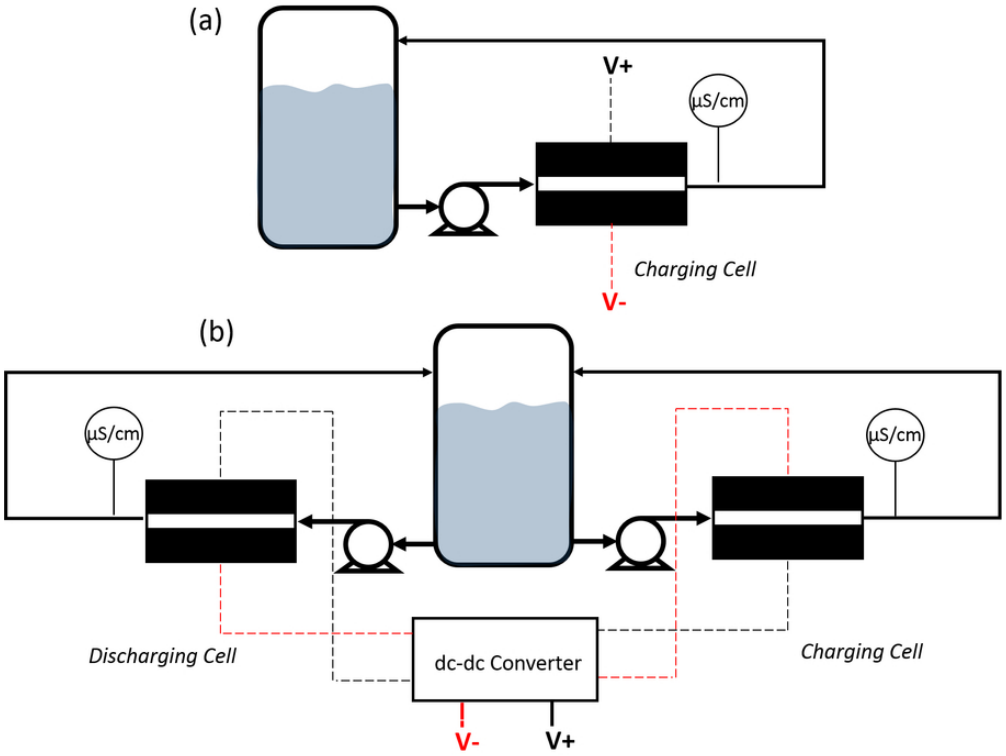

Figure 2. Characterization (a) and energy recovery (b) system configurations for evaluation of desalination and recovery performance in the i-CDI and i-MCDI cells.

77x60mm (300 x 300 DPI)

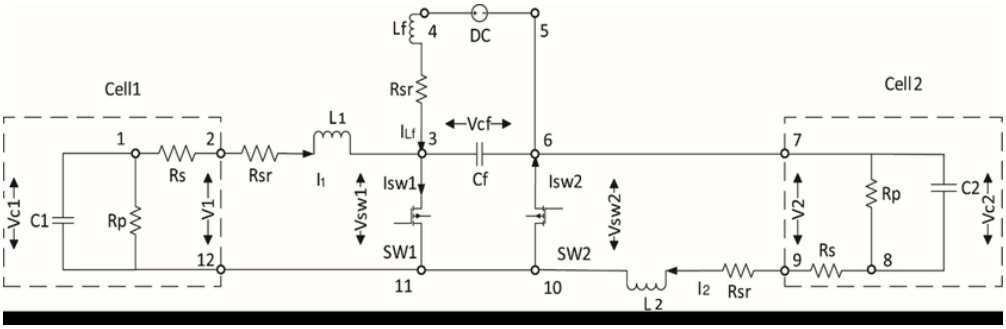

Figure 3. Circuit diagram of the dc-dc converter energy recovery system.

71x22mm (300 x 300 DPI)

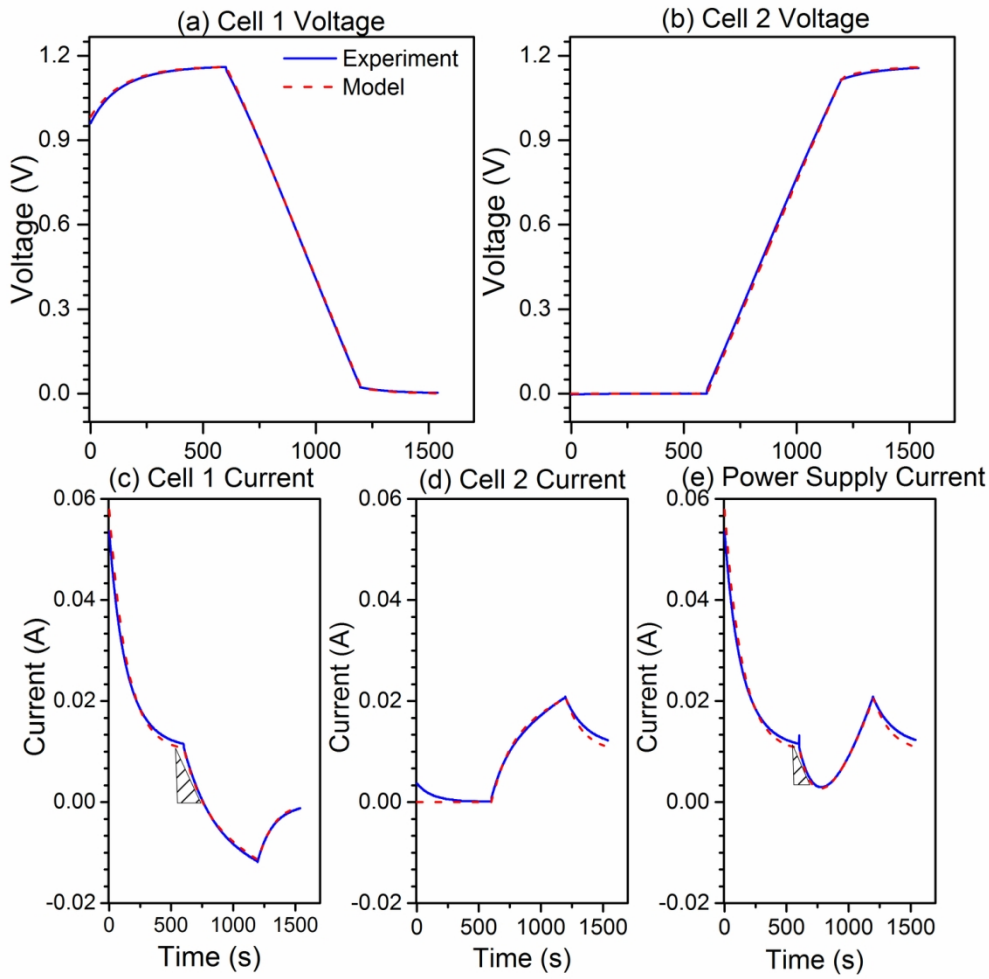

Figure 4. Voltage profiles for cell 1 (a) and cell 2 (b), in addition to current profiles for cell 1 (c), cell 2 (d), and the power supply (e) during constant voltage pre-charging and energy recovery using the dc-dc converter system with the EDC. The voltage drop and ramp time during the recovery phase were 0 V and 600 s, respectively. The power supply output voltage was constant at 1.2 V.

132x132mm (300 x 300 DPI)

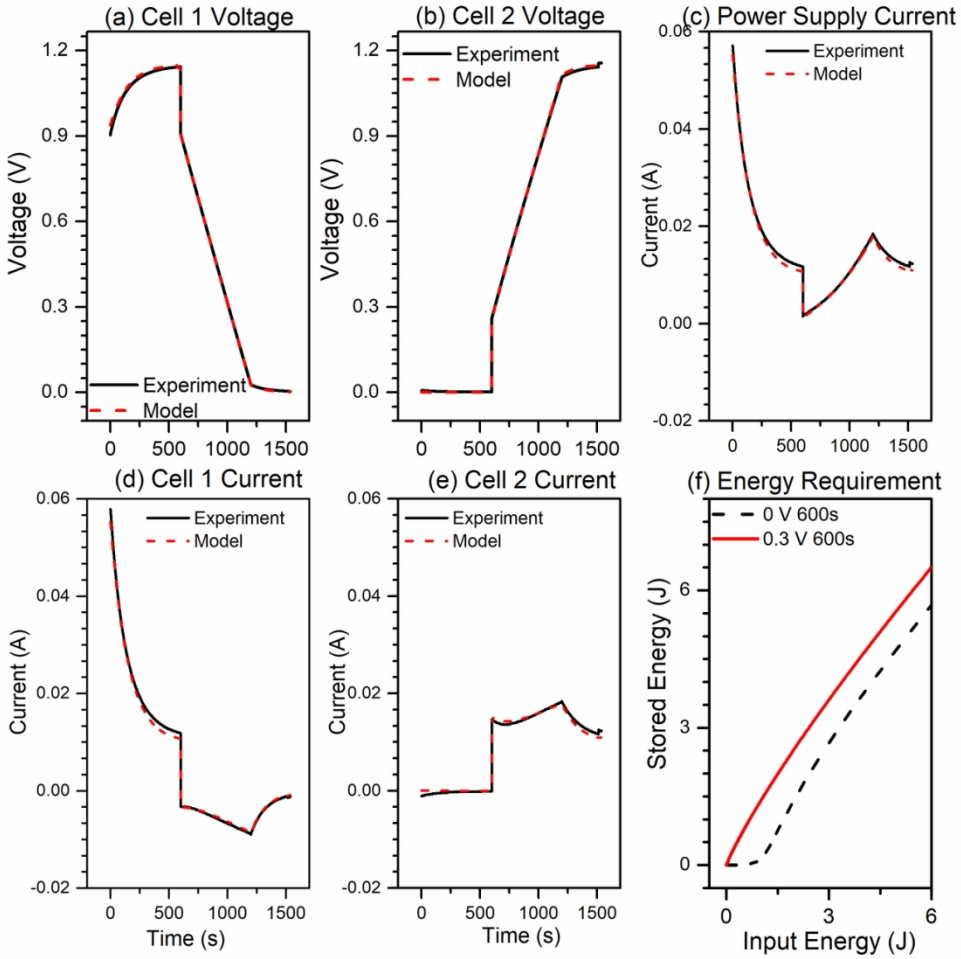

Figure 5. Voltage profiles for cell 1 (a) and cell 2 (b), power supply current (c), and current profiles for cell 1 (d) and cell 2 (e) during constant voltage pre-charging and energy recovery using the dc-dc converter system with the EDC. The voltage drop and ramp time during the recovery phase were 0.3 V and 600 s, respectively. The power supply output voltage was constant at 1.2 V. Energy requirements for constant voltage (1.2 V) and recovery-aided charging with and without an initial voltage drop are shown in (f).

114x114mm (300 x 300 DPI)

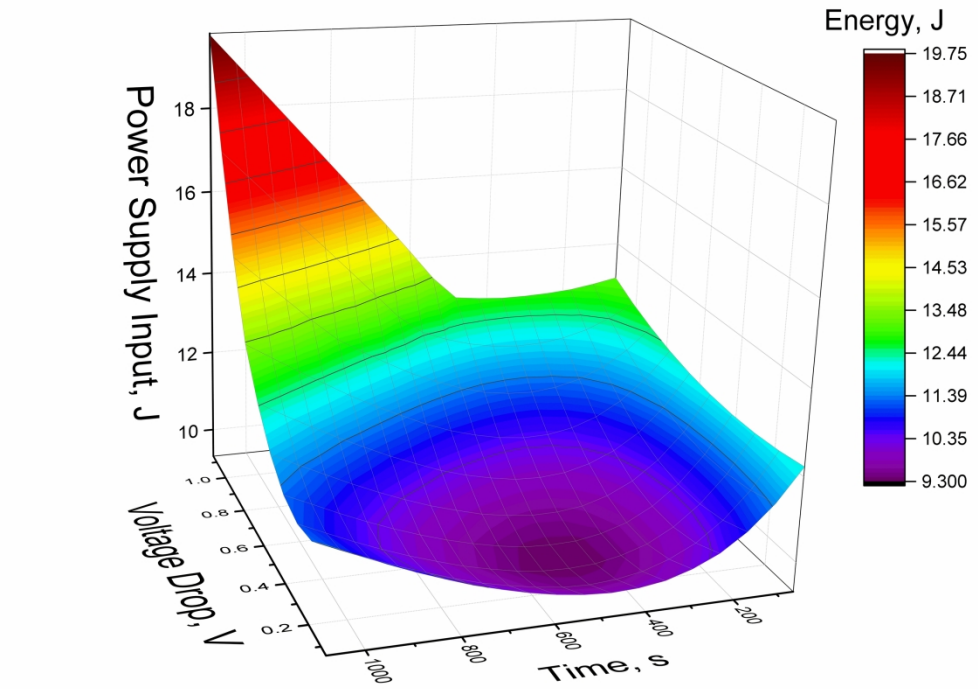

Figure 6. Power supply energy input requirement to charge cell 2 during the recovery step as a function of initial voltage drop and ramp time, preceded by charging cell 1 at constant voltage for 600 s.

272x208mm (300 x 300 DPI)

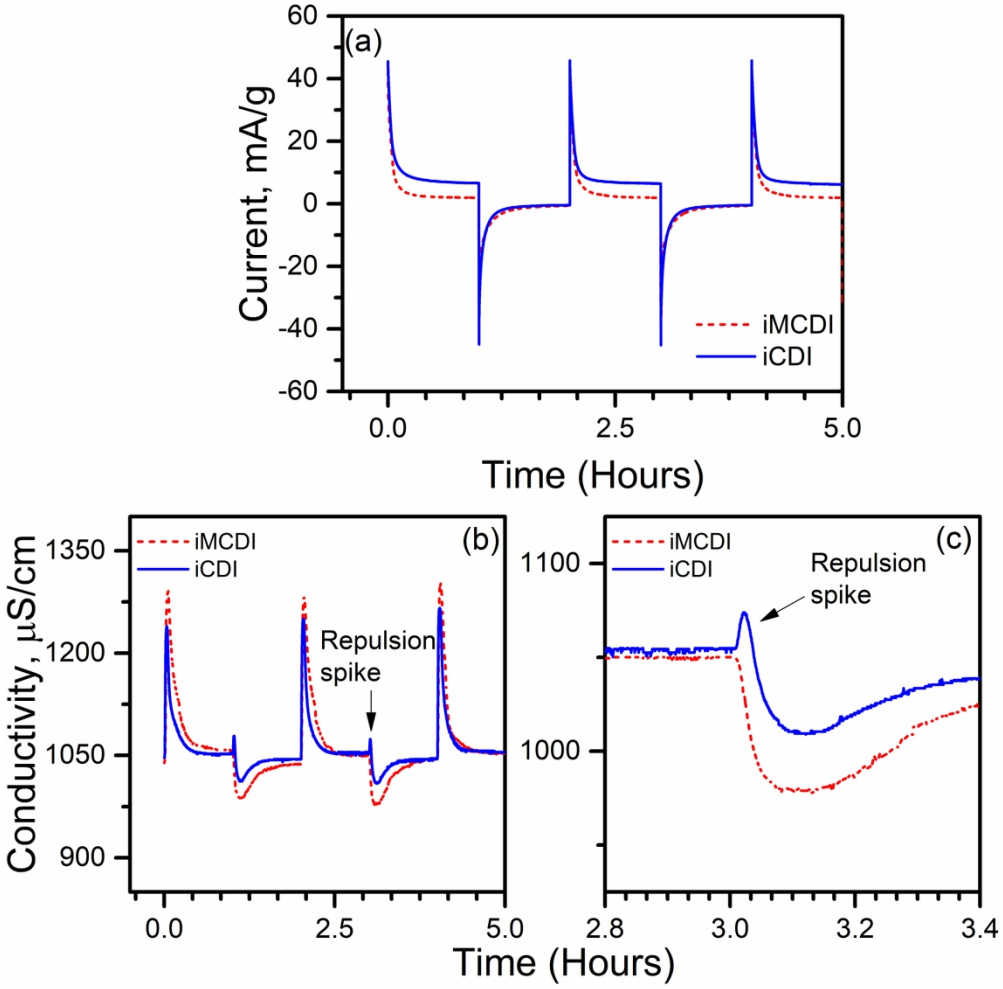

Figure 7. Current (a) and conductivity (b) zoomed-in conductivity profiles for charging and discharging operation of an i-CDI and i-MCDI cell. Performance testing was conducted by charging/ (1.2 V) and depolarizing (short-circuit) a 18.5 L volume of a ~10 mM NaCl stream recirculating at ~14 ml/min in the test cell.

203x203mm (300 x 300 DPI)

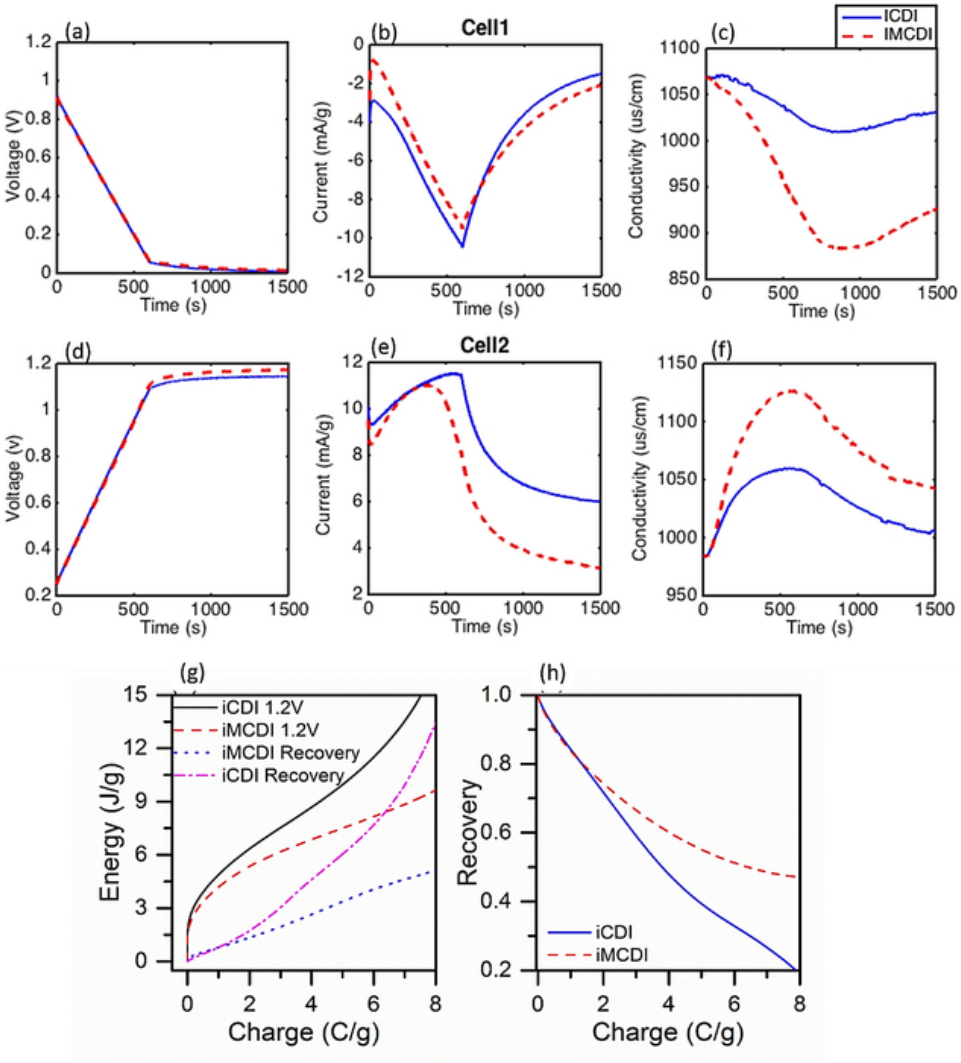

Figure 8. Voltage, current, and conductivity profiles during the energy recovery process. Profiles for cell 1 are shown in (a-c), and for cell 2 in (d-f). Energy cost (g) and recovery (h) on an ion charge basis are compared to the constant voltage requirements.

55x59mm (300 x 300 DPI)

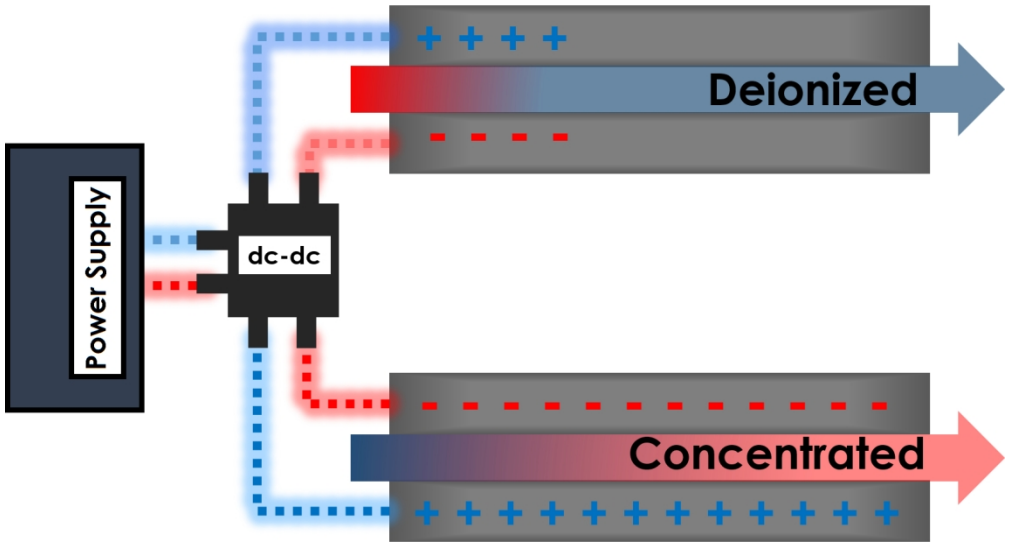

451x260mm (96 x 96 DPI)